Organic Electronics 13 (2012) 525–531

Contents lists available at SciVerse ScienceDirect

Organic Electronics

journal homepage: www.elsevier.com/locate/orgel

High performance hybrid near-infrared LEDs using benzenedithiol cross-linked PbS colloidal nanocrystals

Xin Ma [a], Fan Xu [a], Jaime Benavides [a], Sylvain G. Cloutier [a,b,*]

[a] Department of Electrical and Computer Engineering, University of Delaware, Newark, DE, USA
[b] Département de Génie Électrique, École de Technologie Supérieure, Montréal, QC, Canada

ARTICLE INFO

Article history:
Received 29 October 2011
Received in revised form 2 December 2011
Accepted 23 December 2011
Available online 7 January 2012

Keywords:
Near-infrared light emitting diodes
Hybrid heterojunctions
Colloidal nanocrystals
Nanocrystalline solids
Bezenedithiol
Ligand-exchange

ABSTRACT

We report an all solution-based processing method to produce efficient hybrid polymer–nanocrystal multilayered heterostructures for electroluminescence in the near-infrared (1050–1600 nm). We employ for the first time the benzenedithiol cross-linking method to produce high-quality PbS nanocrystalline films acting both as an electron-transporting and electroluminescent layer within a near-infrared light emitting diode (LED) architecture. Due to the large volume of nanocrystals and the good carrier-transport properties within the cross-linked nanocrystalline films, this device architecture yields high emission powers and good quantum efficiencies. In contrast, using ethanedithiol cross-linking molecules results in nanocrystalline films with low photo- and electro-luminescence efficiencies.

1. Introduction

The synthesis of exotic lead-chalcogenide nanostructures and their self-assembly into more complex monolayers (2D) and nanocrystalline film structures (3D) has created an entirely new paradigm in low-cost and high-performance optoelectronic materials research, largely due to the facile solution-based processing and the large versatility of these structures [1–3]. Recently, the dithiol-based ligand-exchange has enabled high-quality self-assembled PbS and PbSe lead-chalcogenide nanocrystalline film structures [4]. In this ligand-exchange process, short cross-linking molecules producing strong thiolate group on each end are used to replace the oleate capping group around colloidal nanocrystals to achieve the cross-linking of the nanocrystals into films. High structural quality and excellent electronic transport properties have propelled these self-assembled nanocrystalline lead-chalcogenide film structures to the forefront of cutting-edge research in the area of low-cost photovoltaic and photodetector platforms [5–9]. Meanwhile, close-packed and cross-linked CdSe-based nanocrystalline film structures have significantly improved the performances of hybrid light-emitting diodes (LEDs) for the visible [10–12]. However, very few reports have explored the potential use of dithiol-treated lead-chalcogenide nanocrystalline films for near-infrared light emitting diodes (LEDs) architectures. Due to the long oleate capping ligands keeping lead-chalcogenide nanocrystals stable in solution, previously proposed hybrid near-infrared LED structures mostly relied on nanocrystals embedded within a polymer host matrix [13,14], or on a monolayer of nanocrystals sandwiched between organic carrier-transporting layers [15]. In these structures, the low density of nanocrystals and the significant carriers and exciton losses to visible residual emission from the organic layers severely limit the performances of those near-infrared LEDs [13,15].

In this report, we apply a 1,3-benzenedithiol (BDT) cross-linking treatment to achieve an all-solution, robust, and versatile pathway to produce hybrid polymer–nanocrystal multilayered-heterostructure LEDs with high

* Corresponding author. Present address: École de Technologie Supérieure, 1100 rue Notre-Dame Ouest, Montréal, QC, Canada H3C 1K3. Tel.: +1 514 396 8897; fax: +1 514 396 8684.
E-mail address: sylvaing.cloutier@etsmtl.ca (S.G. Cloutier).

1566-1199/$ - see front matter © 2011 Elsevier B.V. All rights reserved.
doi:10.1016/j.orgel.2011.12.012

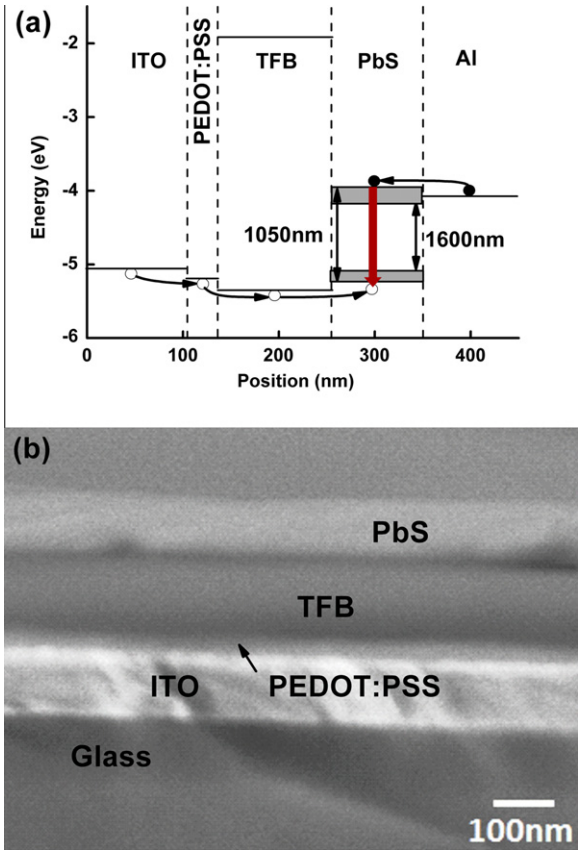

Fig. 1. (a) Energy diagram for the hybrid multilayered LED. The HOMO and LUMO levels for the TFB are obtained from Ref. [16]. The band edges for PbS nanocrystals are obtained from Ref. [17]. (b) Cross-sectional SEM image of device without the top aluminum contact.

near-infrared emission and no residual visible emission. In our multilayered device architecture summarized in Fig. 1, the electron-transporting layer consists of a 100 nm-thick self-assembled PbS nanocrystalline film cross-linked by BDT ligand-exchange treatment that was deposited on top of a hole-transporting polymer film. The nanocrystalline film structure is fabricated using layer-by-layer deposition and ligand exchange treatment to achieve superior structural quality and better charge-transport properties. As we show, the resulting nanocrystalline film provides an efficient electron-transporting and light-emitting structure. In contrast, we observed that another popular dithiol molecule 1,2-ethanedithiol (EDT) leads to poor LED efficiencies in the same device structure. Finally, examining the conductivities and hole mobilities of these dithiol-treated PbS nanocrystalline films provides a deeper understanding of the intricacies associated with those two popular yet complex self-assembly processes using EDT [5,7] and BDT [4,6,9] linkers.

2. Materials and methods

The PbS nanocrystals used in this paper are synthesized using the method pioneered by Hines and Scholes [18]. In a typical synthesis of PbS nanocrystals emitting at 1050 nm, 0.45 g of lead oxide, 10 g of octadecene and 1.34 g of oleic acid are added to a three-neck flask and heated to 80 °C for 2 h under vigorous stirring in low vacuum to degas and dissolve the mixture. Then, the temperature is kept at 120 °C under nitrogen flow for 30 min before a second solution consisting of 105 μl of hexamethyldisilathiane diluted in 4 ml of octadecene is quickly injected into the reaction flask under vigorously stirring. After the completion of the reaction, the colloidal PbS nanocrystals are collected by quick injection of the reaction solution into an excess amount of acetone (with a ratio of 1:4) for centrifugation. To ensure adequate removal of the reaction solvents, precipitation and re-dispersion are repeated multiple times. By using a IR-26 dye solution with a 0.3 optical density (quantum yield of 0.05% [19]) as reference, a 20% quantum yield is estimated for these 1050 nm emitter PbS nanocrystals in solution. Fig. 2 shows the TEM images of different sizes of PbS nanocrystals synthesised by changing the amount of oleic acid (from 1.34 g to 20 g) used in this procedure.

The near-infrared LED device consists of a multilayered structure using indium-tin-oxide (ITO) as the anode, poly(3,4-ethylenedioxythiophene):poly(styrenesulphonate) (or PEDOT:PSS) as the hole injection layer, poly(2,7-(9,9-di-*n*-octylfluorene)-*alt*-(1,4-phenylene-((4-*sec*-butylphenyl) imino)-1,4-phenylene)) (or TFB) as the hole transporting layer, cross-linked PbS nanocrystals as electron transporting and light emitting layer, and aluminum (Al) as the cathode. To prepare the samples, the ITO substrate (R_s = 15–25 Ω, Delta Technologies) is first pre-patterned by photolithography followed by a wet-etching in 20% hydrochloric acid solution. The substrate is then sequentially cleaned in de-ionized water, acetone, and isopropanol ultrasonic baths each for 15 min. The hole-injection layer of PEDOT:PSS (CLEVIOS™ P VP Al 4083) is spin-coated on top of the ITO substrate at 3000 rpm for 90 s and then annealed at 135 °C for 30 min in air. The layer of TFB (American Dye Source, Inc.) is spin-coated atop the PEDOT:PSS film using toluene solutions with different TFB concentrations (8 mg ml^{-1}, 12 mg ml^{-1} and 16 mg ml^{-1}) for thickness optimization. After annealing at 150 °C for 10 min in a nitrogen-purged oven, the TFB film thicknesses is measured to be 60 ± 15, 90 ± 15 and 120 ± 15 nm, respectively for the three concentrations used. Subsequently, a layer-by-layer spin-coating of hexane-based colloidal solutions of PbS nanocrystals (about 10 mg ml^{-1} concentrations) is processed directly atop the TFB. The deposition of each layer of nanocrystals includes 3 steps: (1) spin-coating of the colloidal nanocrystals solution at 2000 rpm for 30 s, (2) deposition of several drops of the 1,3-benzenedithiol (BDT) acetonitrile solution (0.02 M) to fully cover the substrate, wait for 30 s to enable the exchange process before spin-coating for 30 s at 2000 rpm, and (3) rinsing the sample with hexane during spinning to wash away any excess of PbS nanocrystals and BDT residues. Devices with 2, 4, 6, and 8 layers (with roughly 25 nm per layer) of nanocrystals were produced using this method to investigate the optimal electron-transporting layer's thickness. Finally, a 150 nm-thick Al cathode is deposited through a shadow mask by e-beam evaporation at a rate of 1 Å s^{-1}. No further treatment and/or encapsulation is performed on the devices. To avoid trapping states formation at the contact between Al and nanocrystals

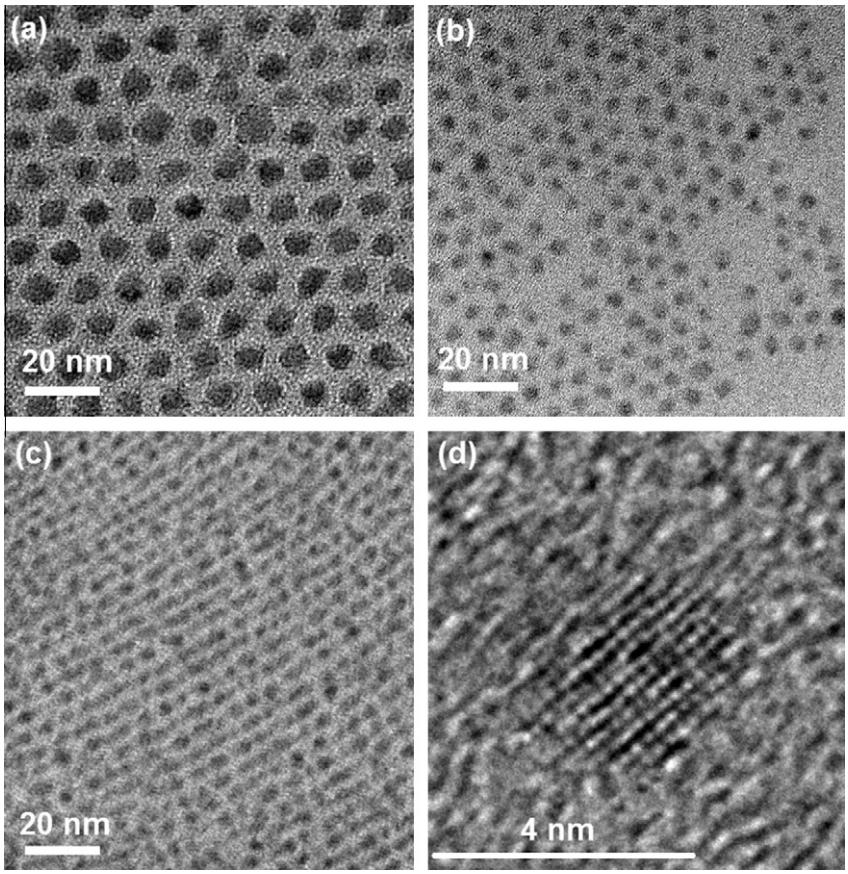

Fig. 2. (a) 7 nm, (b) 5 nm and (c) 3.5 nm PbS colloidal nanocrystals observed under TEM. (d) Lattice structure of a single 3.5 nm nanocrystal under high-resolution TEM (HRTEM).

after long term air exposure [20], all devices are tested within 2 h after fabrication, and no current-drop is observed in this time scale.

The TEM images are obtained using a JEM 2010F instrument operating at 200 KeV. The SEM images are obtained using a JSM-7400F field-emission SEM instrument operating at an acceleration voltage of 3 kV. Photoluminescence (PL) and electroluminescence (EL) spectra are recorded using a Jobin-Yvon iHR320 triple-grating spectrometer equipped with a Symphony thermoelectric-cooled InGaAs CCD array for the near-infrared and a Synapse silicon CCD array for the visible. For photoluminescence excitation, we use a 250 mW frequency-stabilized TORUS (Laser-Quantum Inc.) laser operating at 532 nm. Electroluminescence excitation is performed using a Keithley 236 source-measure unit. The device power–current–voltage (PIV) device characteristics are recorded by placing the device on the port of an integrating sphere coupled to a Newport IR-818 photodetector. The integrating sphere is carefully calibrated using a lambertian GaInN LED. Absorption measurements are performed on a UV–VIS–NIR spectrometer (UV-3600, Shimadzu) and the near-infrared image of the device's emission is collected by Xenicsxeva near-infrared camera coupled to a 2× magnifier. For the measurement of conductivity and hole mobility of the PbS nanocrystalline film by CELIV method, the sample consists of a 250–350 nm-thick nanocrystalline film fabricated using the layer-by-layer spin-coating method sandwiched directly between ITO and Al contact. A linearly-increasing bias is applied using a function generator (Agilent 33220A) at 20 MHz and the transient currents are measured by recording the voltage drop across a 200 Ω resistive load using a digital oscilloscope (Agilent 54621A). All measurements are performed at room temperature.

3. Results and discussion

3.1. Hybrid near-infrared LED structure with BDT linker

As shown in Fig. 3, a TFB polymer-only device with no nanocrystalline film displays a clear single carrier (hole) trap-limited current regime between 1 and 2 V [21], before reaching a quasi space charge-limited current regime with slope $m \approx 2.7$. This single carrier behavior is consistent with the large energy barrier between the HOMO of the TFB and the aluminum cathode for electron injection. For the LED device using the optimized BDT cross-linked nanocrystalline film structure atop the TFB, measurements indicate a high current density at low voltages originating from the efficient electron injection at the nanocrystal–aluminum junction. As shown in Fig. 1(a), the good match between the aluminum cathode's work function and the conduction

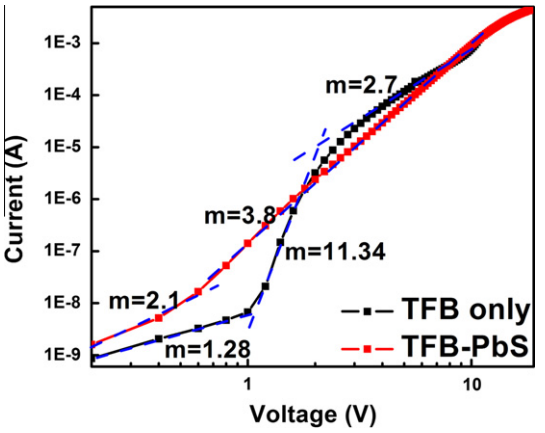

Fig. 3. Current–voltage characteristics for the hybrid multilayered LED using a BDT-treated nanocrystalline film and for a TFB polymer-only control device.

band of the self-assembled nanocrystalline layer offers the convenience of removing additional electron transporting organic and/or low work function metal layers in-between. This precludes additional carrier losses and unwanted visible luminescence, while simplifying the fabrication process and providing better device stability. At the heterojunction between hole-transporting layer and electron-transporting BDT-treated PbS nanocrystalline layer, the low LUMO of the TFB provides a fantastic electron barrier that efficiently confines the electrons within the PbS nanocrystalline film structure and thus prevents any light emission from the polymer layer during device operation.

In Fig. 4, we display the external quantum efficiency (EQE) and output power measurements for devices with different TFB and nanocrystalline film thicknesses. As shown in Fig. 4(a), the EQE and output powers of the devices increase along with increasing the thickness of the hole-transporting TFB layer, while keeping the same 100 ± 15 nm-thick nanocrystalline film's thickness. This is consistent with the dual role of the TFB layer which consists in: (1) providing an efficient electron barrier to confine the injected electrons at the polymer/nanocrystals interface and favor exciton binding, and (2) limiting the excess hole–current flowing through the entire device structure. However, increasing the polymer layer's thickness also increases the device's turn-on voltage from about 2 V for the 60- and 90 nm-thick TFB films to 3.4 V for the 120 nm-thick TFB film.

Based on these results, we decided to use a 120 nm-thick TFB layer for the nanocrystalline layer optimization shown in Fig. 4(b), as it provides the optimal output powers and EQEs. There, multiple spin-coated layers obtained from the same solution of nanocrystals emitting at 1150 nm were used for comparison. Due to a lower photoluminescent efficiency of the 1150 nm emitter nanocrystals, this bath of samples have a lower device EQE than the devices in Fig. 4(a). With each nanocrystals layer being 25 nm-thick, the EQE peaks with devices using 4 layers of nanocrystalline film (100 ± 15 nm thick). For thinner nanocrystalline films (2 layers), the active region is too thin and the metal contact quenching leads to lower EQEs. In thicker structures (4 layers), the exciton diffusion to the contact is reduced,

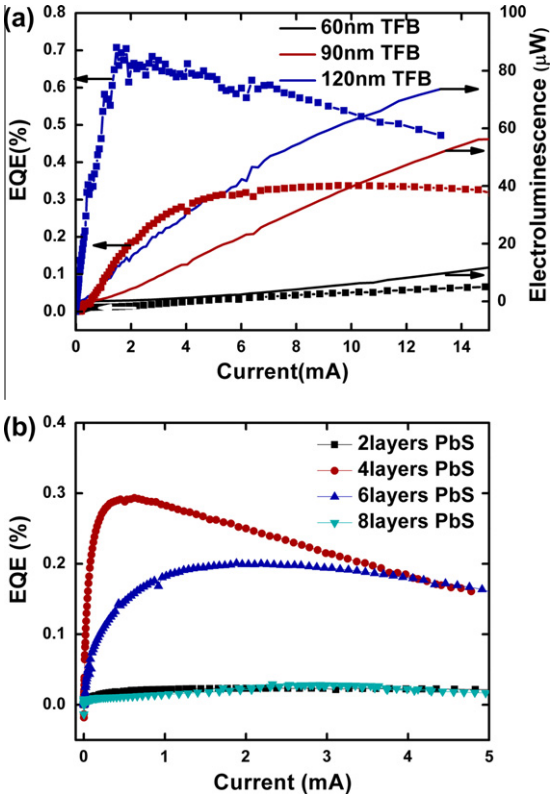

Fig. 4. (a) EQE and emitted power characteristics from samples with different TFB-layer thicknesses. These identical 100 ± 15 nm-thick nanocrystalline film structures all emit at 1050 nm. (b) EQE characteristics from samples with different nanocrystalline film thicknesses using identical 120 nm-thick TFB layer. Each nanocrystal layer is 25 nm-thick. This group of samples operates at 1150 nm. This batch of nanocrystals has a slightly lower photoluminescence efficiency compared with the nanocrystals in (a).

which leads to an increase in radiative recombination. Further increasing the thickness of the nanocrystalline film to 6 and 8 layers results in lower EQEs due to the fact that electrons get trapped in defect states before reaching the polymer/nanocrystalline film interface, thus reducing the carrier balance in the active region. As shown in Fig. 4, this all-solution-processed device architecture can produce 5 mm^2 near-infrared LEDs producing up-to a phenomenal 74 μW output power at 1050 nm and EQE's up-to 0.72%. Meanwhile, no residual visible emission from the hole transporting polymer layer is observed, as shown in Fig. 5(a). Finally, Fig. 5(b) shows that near-infrared LED architectures operating at different emission wavelengths can be produced using PbS nanocrystals of different sizes, demonstrating the versatility of this approach.

3.2. EDT vs. BDT cross-link for LED application

On the choosing of the best dithiol treatment for the LED structure, we noticed significant differences between the nanocrystalline film structures obtained using the BDT-treatment and the more conventional EDT-based cross-linking process. While the EDT treatment is known to work well for photovoltaic devices [5,7,22], it consistently

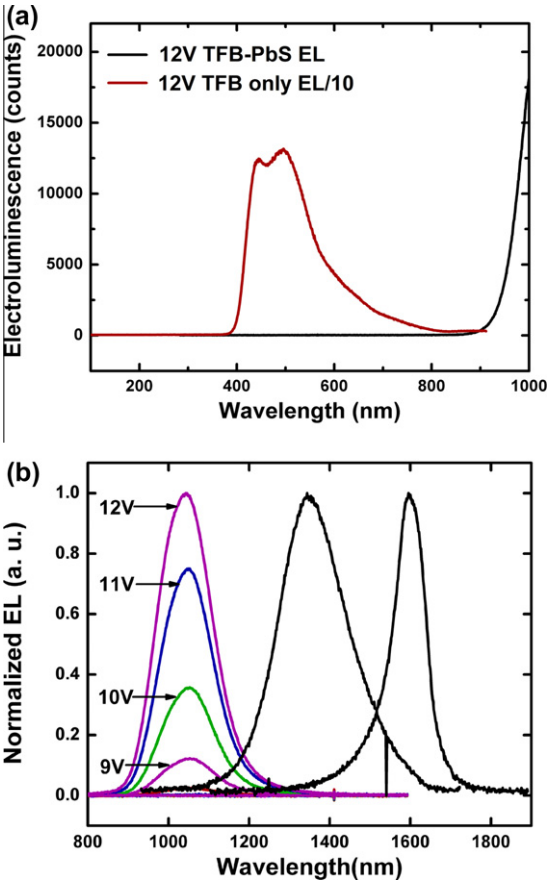

Fig. 5. (a) Visible electroluminescence spectra from a TFB-only LED and a TFB-PbS hybrid LED. While some of the near-infrared emission is seen at the edge of the detection range of silicon CCD array, no TFB emission can be seen from the hybrid LED structure. (b) Normalized electroluminescence spectra for LED structures fabricated from nanocrystalline films using different PbS nanocrystals with emission at 1050, 1350 and 1600 nm, respectively. The narrowing shown on the right shoulder of 1600 nm spectrum is due to InGaAs detector sensitivity cut-off.

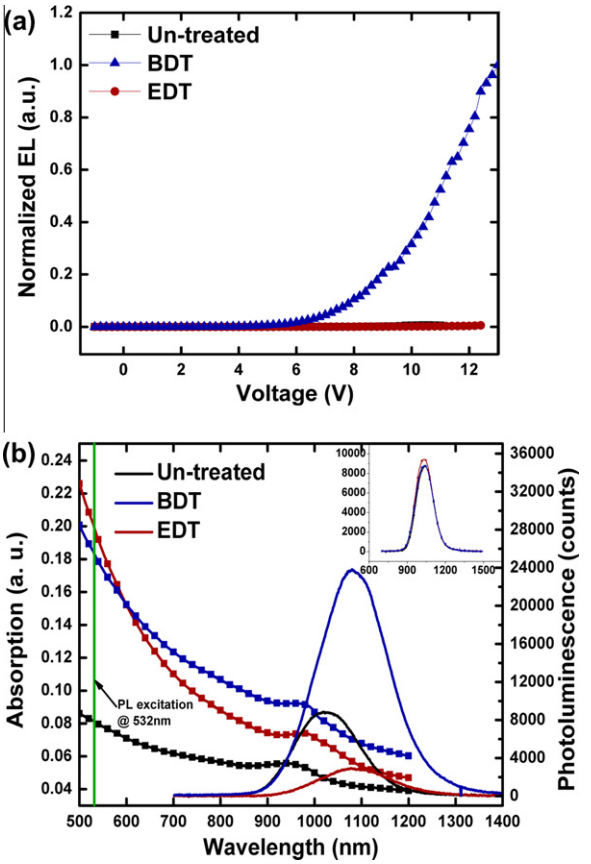

Fig. 6. (a) Power-evolution for the BDT-treated, EDT-treated and pristine un-treated nanocrystalline devices. (b) Absorption (-■-) and photoluminescence (—) for nanocrystalline film structures before and after either an EDT or BDT ligand-exchange treatment. The three samples were produced by spin coating from the same nanocrystal solution under identical conditions. The inset shows the photoluminescence intensities from the three samples before ligand-exchange.

provided us with poor near-infrared LED structures. For example, Fig. 6(a) compares the power–voltage device characteristic of three identical devices with EDT-treated, BDT-treated and pristine un-treated nanocrystalline films. It is clear that the electroluminescence is dramatically lower for the EDT-treated film compared with BDT. In the absorption and photoluminescence spectra shown in Fig. 6(b), the red shifts after both dithiol treatments suggest reduction of quantum confinement and stronger coupling originating from the reduced inter-particle distance following both of these dithiol-based cross-linking treatments [5,23]. While the three samples have the same thick (1 layer, roughly 25 nm), the photoluminescence is significantly higher for the BDT-treated film compared with EDT, which is consistent with the higher electroluminescence consistently observed from the BDT-treated devices. Estimated using the ratio between the absorption at the excitation wavelength and the photoluminescence integral intensities, the relative photoluminescence efficiency for un-treated, BDT, EDT-nanocrystalline films is 1, 1.3 and 0.15, respectively. This shows clearly that although both BDT and EDT cross-linking result in nanocrystalline films with good charge transport properties useful for photodetector and photovoltaic applications [5–9], the distinct improvements in photo- and electro-luminescence efficiency after BDT treatment suggests a significant reduction of non-radiative recombination pathways that is crucial for light-emitting applications.

To further explore the differences between EDT- and BDT-treated nanocrystalline films, we used charge extraction in linearly increasing voltage (CELIV) measurements to obtain the conductivity σ and the majority-carrier mobility μ_h [24,25]. In view of the p-type doping of air-exposed PbS nanocrystalline films, holes are the majority carriers in such films [4]. Using the results from Fig. 7 and the following equations [24]:

$$\sigma = \frac{3d\Delta j}{2t_{\max}A} \tag{1}$$

and

$$\mu_h = \frac{2d^2}{3At_{\max}^2\left(1 + 0.36\frac{\Delta j}{j(0)}\right)} \tag{2}$$

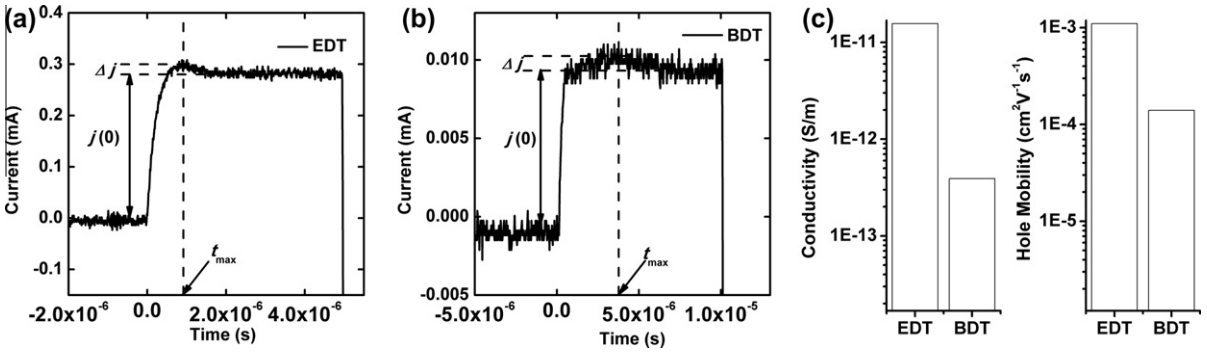

Fig. 7. CELIV transient currents for (a) EDT-treated and (b) BDT-treated nanocrystalline films. For the EDT-treated sample, d = 250 nm and A = 400 kV s^{-1}. For the BDT-treated sample, d = 320 nm and A = 300 kV s^{-1}. (c) Using the parameters obtained from the measurements in (a) and (b), we can obtain 1.56×10^{-11} S $m^{-1}$and 1.1×10^{-3} cm^2 V^{-1} s^{-1} for the conductivity and hole mobility in EDT-treated nanocrystalline films and 3.91×10^{-13} S $m^{-1}$and 1.4×10^{-4} cm^2 V^{-1} $s^{-1}$for BDT-treated nanocrystalline films.

where d is the sample's thickness, A is the increasing-voltage slope, and the parameters t_{max}, Δj and $j(0)$ are obtained from the transient currents shown in Fig. 7(a) and (b), we can obtain directly the conductivity σ and hole-mobility μ_h values summarized in Fig. 7(c). These results indicate that the BDT-treated film has a 40-fold smaller conductivity than the EDT-treated film. Even with an 8-fold smaller hole mobility in the BDT-treated film, this large difference in conductivity suggests a five times lower p-type doping concentration due to less oxidization, most likely resulting from better surface passivation in BDT-treated films. In general, a smaller doping concentration tends to be a desirable thing in LEDs [26]. Moreover, the non-radiative Auger recombination, proportional to the cube of the carrier density, is also the main source of exciton quenching in nanocrystals [27], which makes the low doping level especially desirable for strongly-confined nanocrystalline materials. In contrast, the larger impurity-doping level in the EDT-treated films combined with the faster exciton dissociation rates [23] lead to a large free-carrier density that favors non-radiative processes and quenching of the photo- and electro-luminescence [28].

Finally, the dramatically lower hole mobility in the BDT-treated film also provides a strong mobility barrier that confines the injected holes close to the polymer–nanocrystalline interface to favor the exciton binding. In contrast, the higher hole concentration and hole-mobility in the EDT-treated films lead to hole transport-dominated currents through both the TFB and the nanocrystalline layers, which does not provide the balanced electron and hole densities desirable for LED operation. As such, a better surface passivation, lower doping level, better exciton binding at the hybrid heterojunction interface and balanced carriers injection all combine to offer much better performances in the BDT dithiol-treated LED structure compared with the more conventional EDT treatment.

4. Conclusion

We report an all solution-based processing method producing efficient hybrid polymer–nanocrystal multilayered heterostructures for light-emission in the near-infrared (1050–1600 nm), using a carefully-controlled layer-by-layer BDT cross-linking nanocrystal treatment. After optimization of the hole- and electron-transporting layers thicknesses to 120 and 100 nm, respectively, we obtain near-infrared LEDs with EQEs of 0.72% and up-to 74 μW output power at 1050 nm. The high near-IR emission and no residual visible emission of this device architecture are achieved by using a thick cross-linked nanocrystalline film acting both as the electron-transporting layer and the electroluminescent material. As we show, the good performances of this BDT-treated LED structure compared with the more conventional EDT treatment can be explained by the different surface passivations, doping levels and carrier mobilities resulting from the BDT and EDT treatments. This facile, robust, low-temperature and substrate-independent all solution-processed LED architecture provides a scalable method of producing near-infrared LEDs allowing integration on flexible substrates and amorphous silicon active matrix backplanes [29]. In the future, this LED architecture could be potentially used for flexible and/or reconfigurable integrated opto-electronics, biological imaging and sensing, and lab-on-a-chip platforms [30]. Meanwhile, this approach could also be extended to PbSe colloidal nanocrystal to further extend the LED operation further in the near- and mid-infrared ranges. Finally, the large refractive index of these self-assembled nanocrystalline films also offers the possibility of incorporating electroluminescent structures onto silicon substrates or within more complex device architectures.

Acknowledgements

We would like to thank Sangcheol Kim for the absorption measurements and Dr. Tim Creazzo for the near-infrared imaging. This work was supported under the DARPA COMPASS program through a grant from DOI NBC (N11AP20031) and the AFOSR-DCT program (FA9550-10-1-0363).

References

[1] D.V. Talapin, C.B. Murray, PbSe nanocrystal solids for n- and p-channel thin film field-effect transistors, Science 310 (2005) 86–89.

[2] S.A. McDonald, G. Konstantatos, S. Zhang, P.W. Cyr, E.J.D. Klem, L. Levina, E.H. Sargent, Solution-processed PbS quantum dot infrared photodetectors and photovoltaics, Nat. Mater. 4 (2005) 138–142.
[3] G. Konstantatos, I. Howard, A. Fischer, S. Hoogland, J. Clifford, E. Klem, L. Levina, E.H. Sargent, Ultrasensitive solution-cast quantum dot photodetectors, Nature 442 (2006) 180–183.
[4] J.M. Luther, M. Law, Q. Song, C.L. Perkins, M.C. Beard, A.J. Nozik, Structural, optical, and electrical properties of self-assembled films of PbSe nanocrystals treated with 1,2-ethanedithiol, ACS Nano 2 (2008) 271–280.
[5] G.I. Koleilat, L. Levina, H. Shukla, S.H. Myrskog, S. Hinds, Efficient, stable infrared photovoltaics based on solution-cast colloidal quantum dots, ACS Nano 2 (2008) 833–840.
[6] E.J.D. Klem, H. Shukla, S. Hinds, D.D. MacNeil, L. Levina, E.H. Sargent, Impact of dithiol treatment and air annealing on the conductivity, mobility, and hole density in PbS colloidal quantum dot solids, Appl. Phys. Lett. 92 (2008) 212105.
[7] J.P. Clifford, G. Konstantatos, K.W. Johnston, S. Hoogland, L. Levina, E.H. Sargent, Fast, sensitive and spectrally tuneable colloidal-quantum-dot photodetectors, Nat. Nanotechnol. 4 (2008) 40–44.
[8] H.W. Hillhouse, M.C. Beard, Solar cells from colloidal nanocrystals: fundamentals, materials, devices, and economics, Curr. Opin. Colloid Interf. 14 (2009) 245–259.
[9] K. Szendrei, W. Gomulya, M. Yarema, W. Heiss, M.A. Loi, PbS nanocrystal solar cells with high efficiency and fill factor, Appl. Phys. Lett. 97 (2010) 203501.
[10] K.-S. Cho, E.K. Lee, W.-J. Joo, E. Jang, T.-H. Kim, S.J. Lee, S.-J. Kwon, J.Y. Han, B.-K. Kim, B.L. Choi, J.M. Kim, High-performance crosslinked colloidal quantum-dot light-emitting diodes, Nat. Photonics 3 (2009) 341–345.
[11] W.K. Bae, J. Kwak, J. Lim, D. Lee, M.K. Nam, K. Char, C. Lee, S. Lee, Multicolored light-emitting diodes based on all-quantum-dot multilayer films using layer-by-layer assembly method, Nano Lett. 10 (2010) 2368–2373.
[12] L. Qian, Y. Zheng, J. Xue, P.H. Holloway, Stable and efficient quantum-dot light-emitting diodes based on solution-processed multilayer structures, Nat. Photonics 5 (2011) 543–548.
[13] G. Konstantatos, C. Huang, L. Levina, Z. Lu, E.H. Sargent, Efficient infrared electroluminescent devices using solution-processed colloidal quantum dots, Adv. Funct. Mater. 15 (2005) 1865–1869.
[14] K.R. Choudhury, D.W. Song, F. So, Efficient solution-processed hybrid polymer–nanocrystal near infrared light-emitting devices, Org. Electron. 11 (2010) 23–28.
[15] J.S. Steckel, S. Coe-Sullivan, V. Bulović, M.G. Bawendi, 1.3–1.55 μm tunable electroluminescence from PbSe quantum dots embedded within an organic device, Adv. Mater. 15 (2003) 1862–1866.
[16] J. Hwang, E.-G. Kim, J. Liu, J.-L. Brédas, A. Duggal, A. Kahn, Photoelectron spectroscopic study of the electronic band structure of polyfluorene and fluorene–arylamine copolymers at interfaces, J. Phys. Chem. C 111 (2007) 1378–1384.
[17] B.-R. Hyun, Y.-W. Zhong, A.C. Bartnik, L.-F. Sun, H.D. Abruna, F.W. Wise, J.D. Goodreau, J.R. Matthews, T.M. Leslie, N.F. Borrelli, Electron injection from colloidal PbS quantum dots into titanium dioxide nanoparticles, ACS Nano 2 (2008) 2206–2212.
[18] M.A. Hines, G.D. Scholes, Colloidal PbS nanocrystals with size-tunable near-infrared emission: observation of post-synthesis self-narrowing of the particle size distribution, Adv. Mater. 15 (2003) 1844–1849.
[19] O.E. Semonin, J.C. Johnson, J.M. Luther, A.G. Midgett, A.J. Nozik, M.C. Beard, Absolute photoluminescence quantum yields of IR-26 Dye, PbS, and PbSe quantum dots, J. Phys. Chem. Lett. 1 (2010) 2445–2450.
[20] J. Tang, X.-H. Wang, L. Brzozowski, D.A.R. Barkhouse, R. Debnath, L. Levina, E.H. Sargent, Schottky quantum dot solar cells stable in air under solar illumination, Adv. Mater. 22 (2010) 1398–1402.
[21] Y. Kim, C.-S. Ha, Advances in Organic Light-Emitting Device, Trans Tech Publications, Stafa-Zurich, Switzerland, 2008, p. 29.
[22] J.M. Luther, M. Law, M.C. Beard, Q. Song, M.O. Reese, R.J. Ellingson, A.J. Nozik, Schottky solar cells based on colloidal nanocrystal films, Nano Lett. 8 (2008) 3488–3492.
[23] J.J. Choi, J. Luria, B.-R. Hyun, A.C. Bartnik, L. Sun, Y.-F. Lim, J.A. Marohn, F.W. Wise, T. Hanrath, Photogenerated exciton dissociation in highly coupled lead salt nanocrystal assemblies, Nano Lett. 10 (2010) 1805–1811.
[24] G. Juška, K. Arlauskas, M. Viliūnas, J. Kočka, Extraction current transients: new method of study of charge transport in microcrystalline silicon, Phys. Rev. Lett. 84 (2000) 4946–4949.
[25] G. Juška, M. Viliūnas, K. Arlauskas, N. Nekrašas, N. Wyrsch, L. Feitknecht, Hole drift mobility in μc-Si:H, J. Appl. Phys. 89 (2001) 4971–4974.
[26] A. Zukauskas, M.S. Shur, R. Gaska, Introduction to Solid-state Lighting, John Wiley and Sons Inc., New York, 2002.
[27] V.I. Klimov, A.A. Mikhailovsky, D.W. McBranch, C.A. Leatherdale, M.G. Bawendi, Quantization of multiparticle auger rates in semiconductor quantum dots, Science 287 (2000) 1011–1013.
[28] V.I. Klimov, Optical nonlinearities and ultrafast carrier dynamics in semiconductor nanocrystals, J. Phys. Chem. B 104 (2000) 6112–6123.
[29] T. Rauch, M. Böberl, S.F. Tedde, J. Fürst, M.V. Kovalenko, G. Hesser, U. Lemmer, W. Heiss, O. Hayden, Near-infrared imaging with quantum-dot-sensitized organic photodiodes, Nat. Photonics 3 (2009) 332–336.
[30] B.-R. Hyun, H. Chen, D.A. Rey, F.W. Wise, C.A. Batt, Near-infrared fluorescence imaging with water-soluble lead salt quantum dots, J. Phys. Chem. B 111 (2007) 5726–5730.